PHYSICAL REVIEW D VOLUME 9, NUMBER 5 1 MARCH 1974

Minimal Regge model for meson-baryon scattering: Duality, SU(3), and phase-modified absorptive cuts*

S. E. Egli, D. W. Duke, and N. W. Dean
Institute for Atomic Research and Department of Physics, Iowa State University, Ames, Iowa 50010
(Received 10 September 1973)

A model is presented which incorporates economically all of the modifications to simple SU(3)-symmetric dual Regge-pole theory which are required by existing data on $0^-\frac{1}{2}^+ \to 0^-\frac{1}{2}^+$ processes. The basic assumptions are no-exotics duality, minimally broken SU(3) symmetry, and absorptive Regge cuts phase-modified by the Ringland prescription. We first describe qualitatively how these assumptions suffice for the description of all measured reactions, and then present the results of a detailed fit to 1987 data points for 18 different reactions.

I. INTRODUCTION

The general class of reactions $0^-\frac{1}{2}^+ \to 0^-\frac{1}{2}^+$, where 0^- is a pseudoscalar meson and $\frac{1}{2}^+$ is a spin-$\frac{1}{2}$ baryon, has been studied quite extensively experimentally.[1-48] For lab beam momenta between 3.0 and 65.0 GeV/c, one can describe the main features of this class of reactions near the forward direction in terms of amplitudes dominated by meson Regge trajectories accompanied by the first-order corrections [the Reggeon-Pomeron (RP) cuts], and, in the case of elastic scatterings, a Pomeron contribution. Normally, one calculates the RP cut according to some convolution[49-51] formula.

In contrast with early attempts to fit the high-energy data with Regge poles,[52] recent analyses of the high-energy data have used Regge amplitudes constrained by duality and SU(3), thus avoiding an undesirable (and unnecessary) freedom of parametrization of the amplitudes.[53-58] Even using highly constrained Regge amplitudes does not, of course, solve the problem of calculating the RP cuts accurately.

In order to resolve this problem, we have found it useful to analyze simultaneously a large collection of data for the reaction type $0^-\frac{1}{2}^+ \to 0^-\frac{1}{2}^+$. This amounts to 18 different reactions, with 1987 total data points at lab beam momenta above 3.0 GeV/c. Thus, for the inelastic reactions SU(3) and duality relate the hypercharge- and non-hypercharge-exchange amplitudes, and the Pomeron amplitude used to calculate the RP cuts is highly constrained by the large amount of elastic scattering data. In this way our amplitudes are about as constrained as they can be. Qualitatively, one can see that the data are consistent with a scheme in which the helicity-flip amplitude is not absorbed, the vector-exchange helicity-nonflip amplitude receives a correction which is less destructive in the real part than the absorption model predicts, and the tensor-exchange nonflip amplitude is only slightly absorbed. This picture is consistent not only with the sign of line-reversal breaking in differential cross sections, but with the signs of inelastic polarizations, nearly all of which are entirely cut-induced in our model. For example, in reactions which are exotic according to duality diagrams, the helicity-flip amplitude is purely real and the polarization arises from the imaginary part of the cut. The data are all consistent with a featureless destructive cut in the imaginary part of the vector-exchange amplitude. A destructive cut in the tensor-exchange amplitude contributes to the polarization with the opposite sign. (Throughout this paper we shall use the word "destructive" to imply that an RP cut interferes destructively with the *corresponding Regge-pole term*.)

Recently, a modification of the absorption prescription has been suggested by Ringland *et al.*[55] which has the effects just described: Cuts in tensor-exchange amplitudes are suppressed, and corrections to real parts of vector-exchange amplitudes are small or constructive. Although we use Ringland's prescription in the work to be described, we obtain equally good fits by suppressing tensor-exchange cuts with a strength parameter and rotating (in a crossing-symmetric way) the vector-exchange cut toward the imaginary axis. Evidently, the details of the modifications of absorption-model cuts are not of critical importance so long as (a) cuts in tensor-exchange amplitudes are suppressed, and (b) real parts in vector-exchange cuts are less destructive than in the absorption model.

Section II contains a description of the model used in our analysis. Section III presents some implications that can be drawn from the inelastic polarization data. This discussion does not depend on the specific numerical results of our fit. Section IV explains how the Ringland phase modifica-

tion resolves the conflict between the experimental data and the traditional absorption model. Section V then contains the specific results of our fit to the complete set of data, detailing the mechanisms responsible for the generally good agreement and the disagreement, whenever it exists. Our final amplitudes are presented there, and we compare our model with the recently proposed classical absorption model.[59] Section VI lists our conclusions.

II. DESCRIPTION OF THE MODEL

We have attempted in this analysis to use the constraints of SU(3) and duality to the fullest extent permitted by the data. The Regge-pole part of the amplitude is constructed with SU(3)-symmetric residues satisfying all the constraints of FESR (finite-energy sum rules) duality, including, through factorization, those obtained from the consideration of pseudoscalar-pseudoscalar scattering. Two meson trajectories are used: one for the nonstrange mesons and one for the exchange-degenerate K^*-K^{**} pair. The Pomeron is treated as an ordinary Regge pole with a trajectory of nonzero slope, and is assumed to be a mixture of singlet and octet components. SU(3) is broken only by the inequality of the strange and nonstrange trajectories and by the octet part of the Pomeron. Absorptive corrections to the helicity-nonflip amplitudes are calculated by performing the usual convolution[51] of Regge poles with the Pomeron after the phase modification suggested by Ringland has been applied. Corrections to the Pomeron amplitude are made by including the first two terms in the eikonal expansion.[50]

A. SU(3) details

Work with SU(3)-symmetric residues can be greatly simplified by using a representation of Clebsch-Gordan coefficients in terms of quark wave functions for the particle states. We use the notation $|8,i\rangle$ $(i=1,2,\ldots,8)$ for single-particle octet states and $|8_s,i\rangle$ and $|8_a,i\rangle$ for symmetric and antisymmetric two-particle octet states. Defining eight 3×3 matrices according to $|8,i\rangle = (M_i)_{jk}\,|q_j\bar{q}_k\rangle$, one can derive the following representation for the Clebsch-Gordan coefficients:

$$\langle 8a;\,8b\,|\,8_s\,c\rangle = (\tfrac{3}{10})^{1/2}\langle \tilde{M}_c\{M_a,M_b\}\rangle\,, \tag{1}$$

$$\langle 8a;\,8b\,|\,8_a\,c\rangle = -\frac{1}{\sqrt{6}}\langle \tilde{M}_c[M_a,M_b]\rangle\,. \tag{2}$$

On the right-hand side, angular brackets $\langle\ \rangle$ imply taking the trace and a tilde implies transposition; $\{\ \}$ and $[\ ]$ imply anticommutator and commutator, respectively. Coupling of two octets to the singlet states is given by

$$\langle 8a;\,8b\,|\,1\rangle = -\frac{1}{4\sqrt{2}}\langle\{M_a,M_b\}\rangle\,. \tag{3}$$

One also derives the following useful results:

$$\sum_{i=1}^{8}\langle 8a;\,8b\,|\,8_a\,i\rangle\langle 8c;\,8d\,|\,8_a\,i\rangle = -\tfrac{1}{8}\langle[\tilde{M}_a,\tilde{M}_b][M_c,M_d]\rangle\,, \tag{4}$$

$$\sum_{i=1}^{8}\langle 8a;\,8b\,|\,8_s\,i\rangle\langle 8c;\,8d\,|\,8_s\,i\rangle = \tfrac{3}{10}\langle\{\tilde{M}_a,\tilde{M}_b\}\{M_c,M_d\}\rangle - \tfrac{1}{10}\langle\{\tilde{M}_a,\tilde{M}_b\}\rangle\langle\{M_c,M_d\}\rangle\,, \tag{5}$$

$$\sum_{i=1}^{8}\langle 8a;\,8b\,|\,8_a\,i\rangle\langle 8c;\,8d\,|\,8_s\,i\rangle = \frac{1}{2\sqrt{5}}\langle[\tilde{M}_a,\tilde{M}_b]\{M_c,M_d\}\rangle\,. \tag{6}$$

For mesons, these traces have direct interpretations as quark diagrams.[60] For example, the term

$$\langle\tilde{M}_b\tilde{M}_aM_cM_d\rangle = (M_b)_{ji}(M_a)_{kj}(M_c)_{kl}(M_d)_{li}$$

may be diagrammed as in Fig. 1. For baryons, we write the quark wave functions as

$$|8,i\rangle = (B_i)_{jkl}\,|q_jq_kq_l\rangle$$

and make the replacement

$$(M_i)_{jk} = \frac{1}{\sqrt{2}}(B_i)_{jrs}\epsilon_{krs}$$

in the traces. For calculational purposes, it is convenient to use the 3×3 matrices, even for baryons. A sample trace calculation is given in the Appendix.

Analogous results may readily be derived for couplings involving 10 and 10* as well.

B. The Regge-pole amplitude

The constraints imposed by duality upon the factorizable residues have been worked out previously and we do not repeat them here.[61] The process of obtaining a general expression for the amplitude given the residue contraints is quite easy using the trace methods, since the sum over

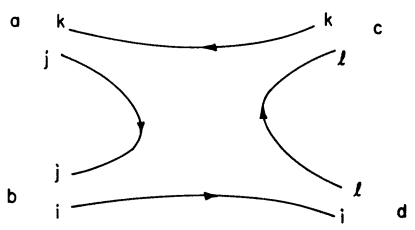

FIG. 1. Quark diagram for four mesons, corresponding to the trace $\langle\tilde{M}_b\tilde{M}_aM_cM_d\rangle$.

t-channel exchanges for a general set of external particles can be done with Eqs. (4)–(6). Using the s-channel helicity amplitudes of Cohen-Tannoudji *et al.*,[62] we obtain

$$\langle cd|T|ab\rangle = (-t)^{|\lambda_a-\lambda_b|/2}\{[\langle \tilde{d}a\,\tilde{c}\,b\rangle (D+F)_{\lambda_a\lambda_b} + (\langle \tilde{d}b\,a\tilde{c}\rangle - \langle \tilde{d}b\rangle\langle \tilde{c}a\rangle)(D-F)_{\lambda_a\lambda_b}] + [\langle \tilde{d}\,\tilde{c}\,ab\rangle (D+F)_{\lambda_a\lambda_b} + (\langle \tilde{d}b\,\tilde{c}a\rangle - \langle \tilde{d}b\rangle\langle \tilde{c}a\rangle)(D-F)_{\lambda_a\lambda_b}]e^{-i\pi\alpha}\}\left(\frac{s}{s_0}\right)^{\alpha}. \tag{7}$$

$D(t)$ and $F(t)$ are independent residues corresponding to symmetric and antisymmetric coupling, respectively, at the baryon vertex. $\tilde{d}$, for example, refers to the transpose of M_d, the 3×3 matrix previously defined. In terms of duality diagrams, the traces may be expressed as shown in Fig. 2.

The same methods can be used to derive duality diagrams for other reactions, including some involving decuplets, such as $PB \to PD$.

C. The vacuum exchange amplitude

Since the πN and KN total cross sections differ substantially over the momentum range considered, the Pomeron cannot be regarded as an SU(3) singlet in our model. We take account of this by giving the Pomeron an explicit $I=Y=0$ octet component. Our amplitude is

$$\langle cd|T|ab\rangle = \left(\tfrac{1}{8}\langle \tilde{d}b\rangle\langle \tilde{c}a\rangle P_s - \frac{1}{2\sqrt{5}}\langle [\tilde{d},b]M_8\rangle\langle \{\tilde{c},a\}M_8\rangle P_{8a} + \tfrac{3}{10}\langle \{\tilde{d},b\}M_8\rangle\langle \{\tilde{c},a\}M_8\rangle P_{8s}\right) \times e^{-i\pi\alpha_P/2}\left(\frac{s}{s_0}\right)^{\alpha_P}. \tag{8}$$

M_8 is the matrix corresponding to the $I=Y=0$ octet state, P_s is the residue for the singlet part of the Pomeron, and P_{8s} and P_{8a} are residues for the octet part with symmetric and antisymmetric coupling, respectively, to $\bar{B}B$. In the fit we present in Sec. V, P_{8a} has been omitted entirely; fits including it as a free parameter take it to a very small and unimportant contribution, so we believe that only P_s and P_{8s} are necessary in this amplitude. We have included a small helicity-flip term, also of the structure given in Eq. (8).

For the vacuum cut, we have kept the first two terms in the eikonal expansion, thus getting a contribution of either sign, and we have fitted an over-all multiplicative cut strength. Since each of the Pomeron terms can be written as Ae^{at}, the cut can be evaluated according to[51]

$$Ae^{at}\otimes Be^{bt} = \tfrac{1}{2}\left(\frac{iq}{4\sqrt{s}}\right)\frac{4\pi AB}{s(a+b)}\exp\left(\frac{ab}{a+b}t\right), \tag{9}$$

$$Ae^{at}\otimes Be^{bt}\otimes Ce^{ct} = \tfrac{1}{6}\left(\frac{iq}{4\sqrt{s}}\right)^2\left(\frac{4\pi}{s}\right)^2 \times\frac{ABC}{ab+bc+ac}\exp\left(\frac{abc}{ab+bc+ac}t\right). \tag{10}$$

The Pomeron helicity-flip amplitudes have been omitted from the cuts.

D. The Regge-Pomeron cut amplitude

In the high-energy limit, the absorption prescription for RP cuts gives, for two exponentials, just the result of Eq. (9). Effectively, the Ringland modification amounts to multiplication of the nonrotating part of the pole by i before convolution with the Pomeron. In crossing-symmetric form, one makes the substitution

$$(e^{-i\pi\alpha}+\tau)\left(\frac{s}{s_0}\right)^{\alpha} \to \left[\ln\left(\frac{s}{is_a}\right)\right]^{-1} \times(e^{-i\pi/4}e^{-i\pi\alpha}+\tau e^{i\pi/4})\left(\frac{s}{s_0}\right)^{\alpha}. \tag{11}$$

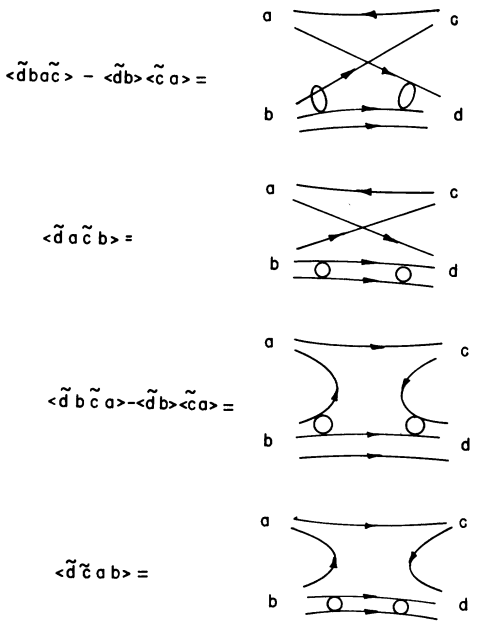

FIG. 2. Quark diagrams for the four traces in Eq. (7). The circles represent antisymmetrized quarks.

We choose s_a to give the multiplicative factor phase $\frac{1}{4}\pi$ at a central energy. For even signature, this change can be written as

$$e^{-i\pi\alpha/2}\cos\frac{\pi\alpha}{2}\to\left[\ln\left(\frac{s}{is_a}\right)\right]^{-1}\times\cos\frac{\pi}{2}(\alpha+\tfrac{1}{2})\,e^{-i\pi\alpha/2}\,. \qquad (12)$$

For odd signature,

$$i\sin\frac{\pi\alpha}{\alpha}\,e^{-i\pi\alpha/2}\to\left[\ln\left(\frac{s}{is_a}\right)\right]^{-1}\times i\sin\frac{\pi}{2}(\alpha+\tfrac{1}{2})\,e^{-i\pi\alpha/2}\,. \qquad (13)$$

We discuss the implications of this modification in a later section.

E. SU(3) breaking

We allow SU(3) breaking only by the octet component of the Pomeron and by trajectory splitting between K^*-K^{**} and the nonstrange mesons. Both of these mechanisms seem to be required by considerations other than detailed fitting of the data, i.e., inequality of the asymptotic πN and KN total cross sections and the positions of mesons on the Chew-Frautschi plot. We have chosen standard values for the trajectory parameters: $\alpha = 0.55 + 0.9t$ for the nonstrange mesons and $\alpha = 0.35 + 0.8t$ for K^*-K^{**}. Our residues all satisfy perfect SU(3).

Of course, the octet part of the Pomeron also contributes to SU(3) breaking in inelastic amplitudes through its appearance in the RP cut. However, the octet part is about 30% of the Pomeron, and the RP cut is typically 25% of the pole, so the effect is not large.

III. QUALITATIVE IMPLICATIONS OF POLARIZATION DATA

Before discussing the model further, we attempt to draw from the inelastic polarization data some inferences which are more general than the results of an explicit fit. This analysis involves the following assumptions:

(1) The phase of the cut varies slowly with t, so neither the real nor imaginary part changes sign in the region of interest.

(2) The helicity-flip amplitude satisfies strong exchange degeneracy.

(3) $(F/D)_{++} < -1$ and $(F/D)_{+-} \approx \frac{1}{3}$ for all $|t| \lesssim 1$, where the subscripts refer to s-channel helicities.

These conditions are all satisfied in our model.

We now examine several reactions individually.

A. $\pi^- p \to \pi^0 n$

In this reaction, only the ρ is exchanged, and the the sign of the polarization is given by

$$P \sim \sin^2\frac{\pi\alpha}{2}\left[1-\left(\frac{\mathrm{Re}}{\mathrm{Im}}\right)_c\cot\frac{\pi\alpha}{2}\right],$$

where $(\mathrm{Re}/\mathrm{Im})_c$ is the real-to-imaginary ratio for the ρP cut, and we have assumed that the imaginary part is destructive of the pole. If the polarization is not to change sign in the region $t > -0.6$, the condition $(\mathrm{Re}/\mathrm{Im})_c < \tan(\pi\alpha/2)$ must be satisfied. Since $(\mathrm{Re}/\mathrm{Im})_c$ is assumed to vary slowly with t while $\tan(\pi\alpha/2)$ decreases rapidly away from $t=0$, we conclude that $(\mathrm{Re}/\mathrm{Im})_c$ must be small, even at $t=0$. The absorption model can accomplish this only with a Pomeron trajectory of large slope which is difficult to reconcile with the elastic differential cross-section data. We conclude that the charge-exchange polarization data is one bit of evidence for a ρP cut which is destructive and more imaginary than in the absorption model.

B. $K^- p \to \pi^- \Sigma^+$

Reactions such as this one, being exotic according to duality diagrams, are useful to consider because the helicity-flip amplitude is purely real, and the polarization therefore isolates the imaginary part of the cut.

Given the assumed values for the F/D ratios, the polarization in this reaction takes the sign $P \sim \mathrm{Im}(K^{**}\otimes P) - \mathrm{Im}(K^*\otimes P)$, where the terms are intrinsically positive if destructive of the pole. The measured polarization is negative, which indicates that the imaginary part of K^* receives a greater destructive correction than does K^{**}. In fact, since a destructive K^{**} cut gives a positive contribution to the $K^- p \to \pi^- \Sigma^+$ polarization, the rather large magnitude of the polarization in this reaction may be taken as evidence for a very small destructive, or even constructive, correction to the imaginary part of K^{**}.

These conclusions also apply to the exotic reactions $K^- n \to \pi^- \Lambda$ and $K^- p \to \pi^0 \Lambda$. In both cases, the polarization is large and its sign indicates a more destructive cut in K^* than in K^{**}.

C. $\pi^- p \to \eta n$

From the polarization in this reaction, we can probably conclude that the systematics of the $A_2 \otimes P$ cut are different from those of $\rho \otimes P$. A destructive, predominantly imaginary cut in the A_2 helicity-nonflip amplitude gives negative polarization, while the measured values are nearly all positive.

D. KN charge exchange

Although experimental data on these reactions are not yet available, they are of particular interest here because they provide rather stringent tests of our basic hypotheses. Our assumptions lead to a strong prediction in the case of K^+n charge exchange. The helicity-flip amplitude should be purely real, and a destructive $\rho\otimes P$ cut gives positive polarization over the entire region $t \gtrsim -1$ (GeV/c)^2.

For K^-p charge exchange, we expect the polarization to arise primarily from the destructive imaginary part of the $\rho\otimes P$ cut, in which case the polarization has the sign $P \sim -\cos\pi\alpha$. Thus, we predict negative polarization, at least for $t \lesssim -0.1$ (GeV/c)^2.

IV. QUALITATIVE FEATURES OF THE MODEL

Having obtained from the data some fairly direct information on certain features of the cuts, we now discuss the qualitative nature of absorption as given by our model. In particular, we show how the Ringland phase modification makes the absorption model consistent with the conclusions reached in Sec. III.

For the purpose of drawing qualitative conclusions, we replace the logarithmic factor $[\ln(s/is_a)]^{-1}$ in Eqs. (12) and (13) with $e^{i\pi/4}$, which is approximately justified over a wide energy range. The statements we make below are all verified by exact calculations.

When the above approximation is made, the cut in the vector-exchange amplitude is obtained by convoluting

$$e^{i\pi/4}\left[-i\sin\frac{\pi}{2}(\alpha+\tfrac{1}{2})\,e^{-i\pi\alpha/2}\right]\left(\frac{s}{s_0}\right)^{\alpha} \tag{14}$$

with the Pomeron. If the Pomeron slope is small ($\alpha_P' \approx 0.3$), we can neglect the real part of the Pomeron for our present purposes. The major contribution to the convolution integral comes from the small-t region because of the exponential decrease of the amplitudes, so the phase of the cut is given roughly by

$$V\otimes P \sim i\,e^{-i\pi(\alpha_0-1/2)/2}\,. \tag{15}$$

For the nonstrange exchanges ($\alpha_0 = 0.55$), the cut is destructive and almost purely imaginary.

For K^* ($\alpha_0 = 0.35$) the situation is not quite as simple. The lower intercept causes a constructive real part to arise in addition to the destructive imaginary part. Were we to multiply the nonrotating part of the pole by $e^{i\pi\alpha_0}$ rather than i, greater symmetry between the cases of strangeness exchange and nonstrangeness exchange would result; the K^* cut would also be nearly purely imaginary. To investigate the importance of the constructive real part in the K^* cut, consider

$$\left(\frac{d\sigma}{dt}\right)_{\rm R} \sim |[K^{**}+(K^{**}\otimes P)]+[K^*+(K^*\otimes P)]\,|^2\,,$$

$$\left(\frac{d\sigma}{dt}\right)_{\rm NR} \sim |[K^{**}+(K^{**}\otimes P)]-[K^*+(K^*\otimes P)]|^2\,.$$

Here NR refers to a reaction with a purely real ("nonrotating") pole amplitude and R refers to its line-reversed ("rotating") counterpart, with phase $e^{-i\pi\alpha}$. If we ignore terms quadratic in the cuts, we have

$$\left(\frac{d\sigma}{dt}\right)_{\rm NR}-\left(\frac{d\sigma}{dt}\right)_{\rm R} \sim -2\,{\rm Re}\,[K^{**}(K^*\otimes P)^* + K^*(K^{**}\otimes P)^*],$$

where an asterisk on the cut terms implies complex conjugation. The K^* and K^{**} pole terms have imaginary parts of the same sign and real parts of opposite signs. Thus, we see that for both cuts, positive contributions to the difference come from destructive imaginary parts and constructive real parts. (In the absorption model, the large, destructive real parts of the cuts give the wrong sign for line-reversal breaking; the real parts are overabsorbed.) Qualitatively, therefore, the polarizations we have considered and the signs of line-reversal breaking do not distinguish a vanishing real part in the K^* cut from a constructive one. We find on the basis of χ^2 that the earlier prescription (i rather than $e^{i\pi\alpha_0}$) is somewhat preferred. The constructive real part plays a role in "fine-tuning" the fit to differential cross-section magnitudes, but has no strong qualitative effect. The important point is that the destructive real part, as given by the absorption model, has been modified. Whether it goes to zero or becomes constructive is more a matter of detail and is probably not well decided by our parametrization-dependent fit.

For tensor exchange, we convolute:

$$e^{-i\pi(\alpha-1/2)/2}\cos\tfrac{1}{2}\pi(\alpha+\tfrac{1}{2})\left(\frac{s}{s_0}\right)^{\alpha}. \tag{16}$$

In the case of K^{**}, $\cos\frac{1}{2}\pi(\alpha+\frac{1}{2})$ is not zero near $t=0$, so our previous arguments give the phase

$$K^{**}\otimes P \sim -e^{-i\pi(\alpha_0+1/2)/2}\,. \tag{17}$$

However, $\cos\frac{1}{2}\pi(\alpha+\frac{1}{2})$ is sufficiently smaller than $\sin\frac{1}{2}\pi(\alpha+\frac{1}{2})$ at small t, even for the K^*-K^{**} trajectory, that the K^{**} cut is suppressed relative to K^*. We see from Eq. (17) that $K^{**}\otimes P$ has a constructive imaginary part and destructive real part. However, just as is the case for ${\rm Re}(K^*\otimes P)$, the K^{**} cut plays no essential role in the fit. Its

effect is to increase somewhat the polarization in exotic reactions and to decrease slightly the amount of line-reversal breaking. This is the effect one gets by increasing the imaginary part of $(K^* \otimes P)$ at the expense of the real part, which may indicate the possibility of a vanishing K^{**} cut, with the K^* cut similar to that of the ρ.

For the A_2 amplitude, $\cos\frac{1}{2}\pi(\alpha+\frac{1}{2})$ goes through zero at small t, and our simple arguments cannot be used. Actual calculation shows that the A_2 cut has a very small constructive imaginary part which gives the positive sign for the polarization in $\pi^- p \to \eta^0 n$ and plays no other role.

Thus, we conclude from this section and Sec. III that the cut terms of dominant importance are the destructive imaginary parts in vector exchange. In a qualitative description of a large amount of $0^-\frac{1}{2}^+$ data no other cuts at all are necessary, and in our explicit model fit they are by far of the greatest importance. Ringland's prescription is successful because it modifies the destructive real part in vector exchange as given by the absorption model and decreases the magnitude of tensor-exchange cuts.

Our results are in disagreement with the dual absorption model, since we do not find peripheral imaginary parts for tensor-exchange amplitudes.[58]

V. DETAILS OF THE FIT

We turn now to a more detailed examination of the model. First we give the explicit parametrization and then discuss the comparison with the data.

A. Parametrization of the model

Using the notation of Eq. (7), we have for the helicity-nonflip Regge residues

$$D+F=(A_1+A_2t+A_3t^2)\,e^{at},$$

$$D-F=Be^{bt}\ .$$

For the helicity-flip residues,

$$D+F=\Gamma(1-\alpha)\,Ce^{ct},$$

$$D-F=\Gamma(1-\alpha)\,De^{ct}.$$

The Pomeron parameters are defined in the notation of Eq. (8):

$$P_s(t)=P_1\exp(p_1t)+P_2\exp(p_2t)\ ,$$

$$P_{8s}(t)=P_3\exp(p_3t)$$

for the nonflip residues, and

$$P_s(t)=P_4\exp(p_4t)\ ,$$

$$P_{8s}(t)=\frac{P_3P_4}{P_1+P_2}\exp(p_4t)$$

for the flip residues.

TABLE I. Parameters determined by the fit presented in Sec. V.

$A_1=-0.537$	$P_1=-9.589$
$A_2=-2.031$	$P_2=-3.181$
$A_3=-2.330$	$P_3=-2.480$
$a=1.154$	$P_4=-1.078$
$B=1.096$	$p_1=2.625$
$b=2.220$	$p_2=-0.314$
$C=1.342$	$p_3=3.306$
$D=0.653$	$p_4=2.877$
$c=0.941$	$\alpha'_P=0.294$
$C_r=0.325$ [a]	$C_P=1.439$

[a] Due to our normalization convention and our method of implementing SU(3) breaking by the Pomeron [Eq. (8)], one should multiply C_r by approximately 4 to facilitate comparison with other works (e.g., Refs. 55–57).

The Pomeron trajectory function is written as $\alpha_P=1+\alpha'_Pt$. Two multiplicative cut strengths were varied in the fit: C_P for the vacuum cut and C_r for the RP cut. Parameter values are given in Table I.

Observable quantities are related to our amplitudes as follows: total cross section

$$\sigma_T=\frac{2\pi^2(0.3893)}{q\sqrt{s}}\,\mathrm{Im}A_{++}(t=0);$$

differential cross section

$$\frac{d\sigma}{dt}=\frac{(0.3893)\,\pi^3}{4q^2s}\,(|A_{++}|^2+|A_{+-}|^2);$$

polarization

$$P=2\,\mathrm{Im}\,(A_{++}A_{+-}^*)/(|A_{++}|^2+|A_{+-}|^2),$$

$$R=\frac{-\cos\theta(|A_{++}|^2-|A_{+-}|^2)+2\sin\theta\,\mathrm{Re}(A_{++}A_{+-}^*)}{|A_{++}|^2+|A_{+-}|^2},$$

$$A=\frac{\sin\theta(|A_{++}|^2-|A_{+-}|^2)+2\cos\theta\,\mathrm{Re}(A_{++}A_{+-}^*)}{|A_{++}|^2+|A_{+-}|^2},$$

where q is the magnitude of the initial center-of-mass momentum, s is the square of the center-of-mass energy, and θ is the laboratory recoil angle of the final-state baryon.

B. Comparison with the data

1. *Total cross sections (TCS)*

The $\pi^- p$ TCS is well reproduced at all momenta between 5 and 65 GeV/c, never straying further

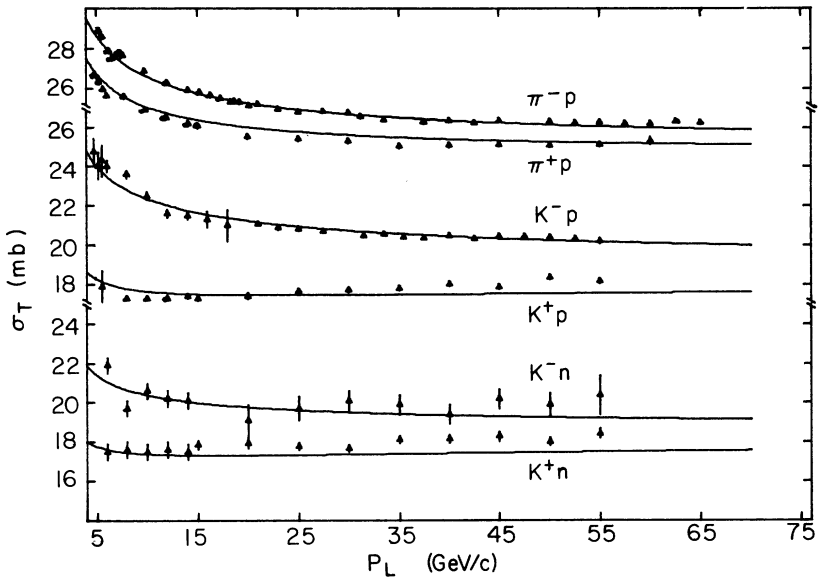

FIG. 3. Experimental measurements (Refs. 1–3, 13, 14, and 19–21) and model results for the total cross sections.

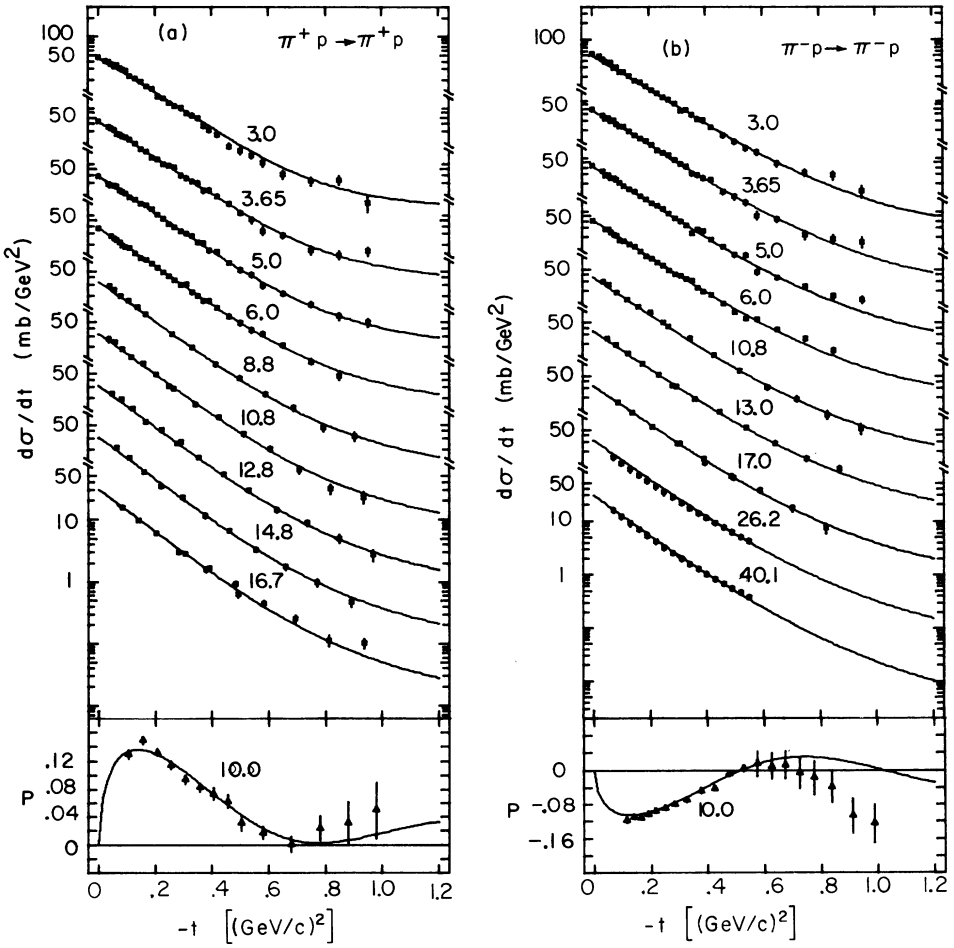

FIG. 4. Experimental measurements and model results for differential cross sections and polarizations. (a) π^+p elastic (Refs. 5–9); (b) π^-p elastic (Refs. 5 and 6). Not all data fitted are shown.

than one third of a millibarn from the data. The π^+p TCS is, however, consistently about half a millibarn higher than the data between 20 and 40 GeV/c. Similarly, the K^-p TCS is fitted very well at all momenta, while the K^+p TCS is somewhat higher than our results at the high momenta. It is actually the TCS differences that are poorly fitted. Since the Pomeron and vacuum cut amplitudes cannot contribute to either TCS difference, the difficulty may be in the energy dependence of the RP-cut contribution. Since the inelastic scattering data are available only over a relatively small energy range, the energy dependence of the RP cut is not well determined in the rest of the fit. We have checked that the discrepancy betwen the model and the data is of the same order of magnitude as the RP-cut contribution, and we conclude that the energy dependence of RP-cut models deserves further study when high-energy inelastic data become available. The total cross sections are shown in Fig. 3.

2. Elastic differential cross sections (DCS)

All the elastic differential cross sections, with the possible exception of K^+p at the lowest energies, are fitted very well at lab momenta above 3.0 GeV/c. In particular, the new high-energy DCS for π^-p and K^-p at 25 and 40 GeV/c are well described in both normalization and t dependence. The model gives a slightly steeper slope to the K^+p DCS than is indicated by the data, but the fit is, in any case, quite satisfactory. The elastic differential cross sections are shown in Figs. 4 and 5.

The new Argonne data at 3.0, 3.65, 5.0, and 6.0 GeV/c provide precise determinations of the DCS differences. Under certain assumptions,[63] one can obtain from these differences the approximate

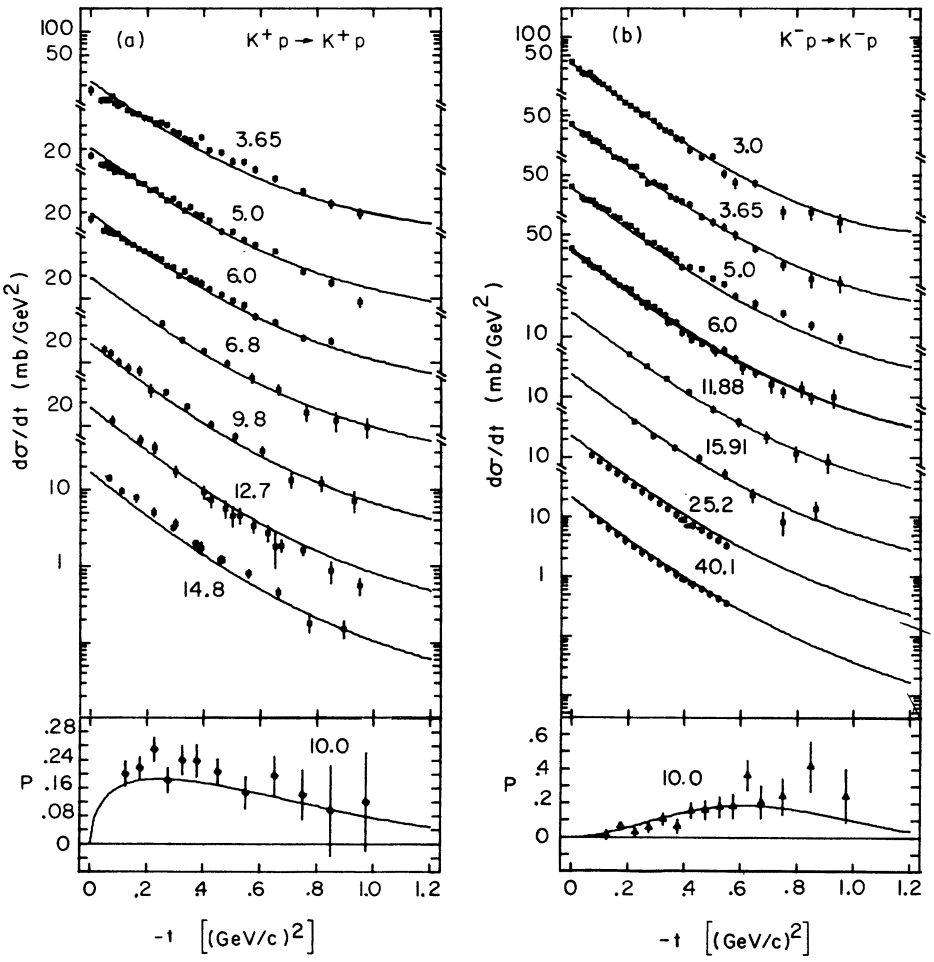

FIG. 5. Experimental measurements and model results for differential cross sections and polarizations. (a) K^+p elastic (Refs. 5, 10, 16, 18, and 22); (b) K^-p elastic (Refs. 5, 10, and 15–18). Not all data fitted are shown.

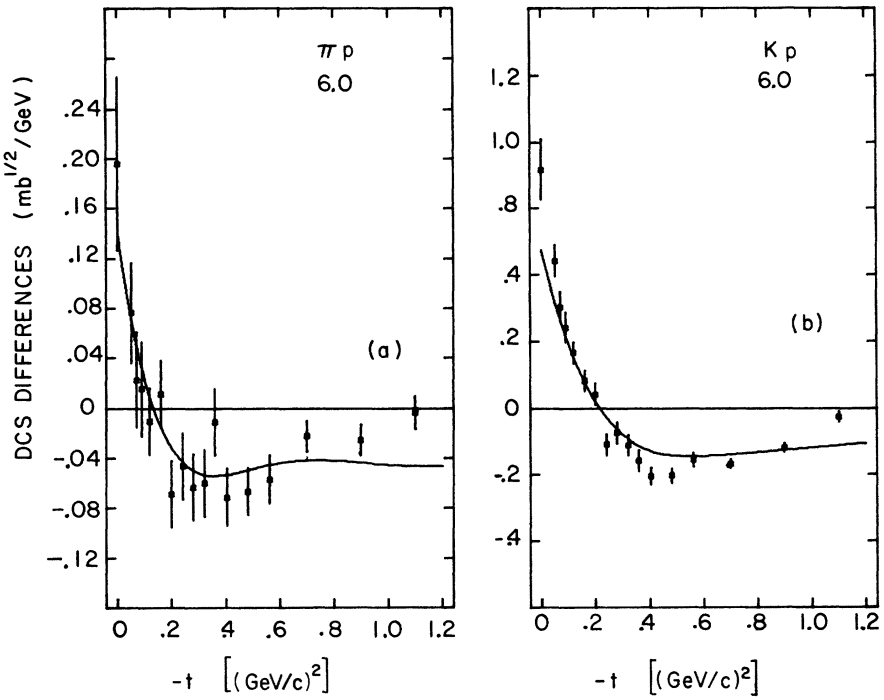

FIG. 6. Experimental (Ref. 5) and model results for elastic differential cross-section differences at 6 GeV/c. (a) $(d\sigma^-/dt - d\sigma^+/dt)/[8(d\sigma^+/dt + d\sigma^-/dt)]^{1/2}$ for πN; (b) the same quantity as in (a) for KN.

imaginary parts of the ρ- and ω- exchange helicity-nonflip amplitudes. In our model, the correct description of the crossover points in KN is due entirely to a very strong RP cut moving the ω- signature zero toward $t=0$. This is direct evidence in favor of the Ringland phase modification for vector $I=0$ exchange. We also note at this point that the primary purpose of the quadratic factor in the helicity nonflip $(D+F)$ is apparently to adjust the relative strength of the RP cut in hypercharge and nonhypercharge exchange reactions. In fact, omitting the quadratic residue results in a πN DCS crossover point closer to $t=0$ than is required by the data, at the expense of a deterioration in the fit to hypercharge-exchange data. The DCS differences are shown in Fig. 6. We have shown in Fig. 7 the effective trajectories determined by our fit compared with the input Pomeron trajectory $\alpha_P = 1 + 0.294t$. The trajectories agree well with the experimentally determined effective trajectories[64] for $t > -1.0$ (GeV/c)^2 (which is the range we fitted), but our model does not reproduce the strong shrinkage exhibited by the larger-t data.[65]

3. *Elastic polarizations*

While the K^+p and K^-p polarizations are well fitted at all energies, there is some disagreement in $\pi^\pm p$ at the lower energies for values of t beyond the ρ- signature zero. In particular, the model exhibits less energy dependence than is present in the data, and prefers the gentler behavior seen at the higher momenta.

Conventionally, the πp polarizations are explained in terms of a flat Pomeron and a ρ-dominated flip amplitude, giving a strong quadratic zero at the wrong-signature point. Although we find complete ρ dominance of the helicity-flip amplitude, the nonzero Pomeron slope causes a splitting of the

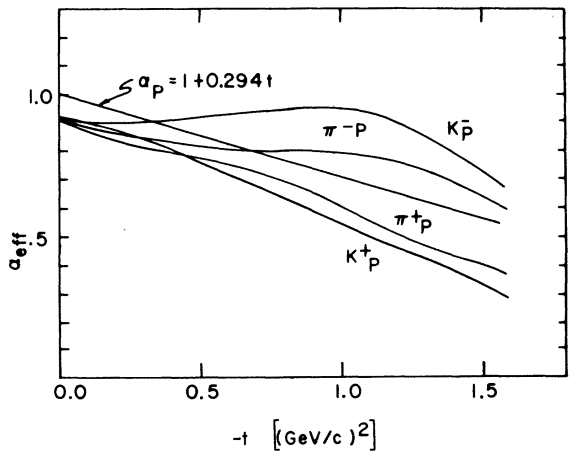

FIG. 7. Model results for the effective $\pi^\pm p$ and $K^\pm p$ trajectories. The straight line is $\alpha_P = 1 + 0.294t$.

quadratic zero into two linear zeros. The vacuum cut only makes matters worse, since it gives a subtractive contribution with more closely spaced linear zeros, causing an even greater separation in the net polarization. The energy dependence of the vacuum-cut phase would require some modification to reproduce the marked double-zero behavior seen at 6 GeV/c. The polarizations are shown in Figs. 4 and 5.

4. Real-to-imaginary ratios, R and A parameters

The real-to-imaginary ratio at $t=0$ for π^+p is fitted very well; however, the corresponding result for π^-p is about a factor 2 too small in magnitude. This result is very sensitive to the t dependence of our residues at small t, and thus is not a major concern.

We have also included R and A for π^-p and R for π^+p in our model fit. Owing to the relative scarcity and uncertainty in these data, they do not influence our amplitudes much in the χ^2 fit. The main conclusion to be drawn from these data is that each of our amplitudes is correct in sign and qualitatively correct in t dependence for $|t| \leq 0.6$ GeV/$c)^2$. These data are the main reason for including a helicity-flip term in the Pomeron amplitude. These data are shown in Figs. 8 and 9.

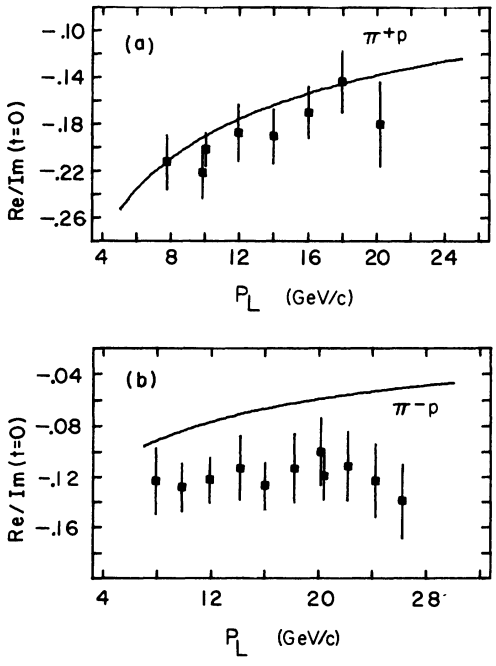

FIG. 8. Experimental measurements (Ref. 4) and model results for the ratio of the real and imaginary parts of the elastic amplitudes at $t=0$. (a) π^+p elastic; (b) π^-p elastic.

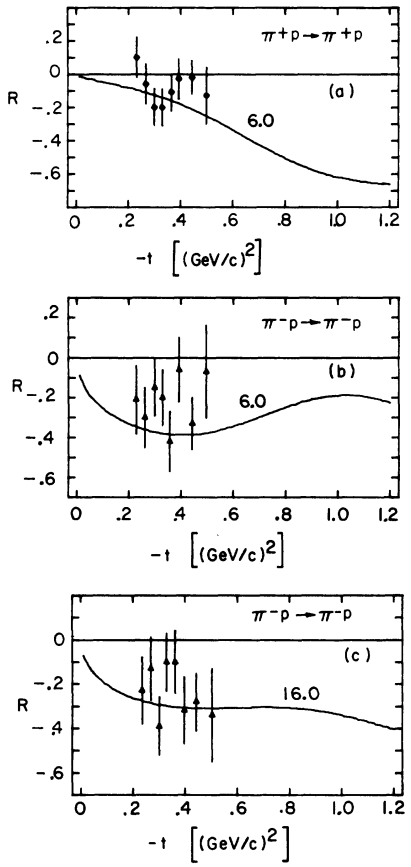

FIG. 9. Experimental measurements and model results for the R parameter (Ref. 12). (a) π^+p elastic at 6.0 GeV/c; (b) π^-p elastic at 6.0 GeV/c; (c) π^-p elastic at 16.0 GeV/c.

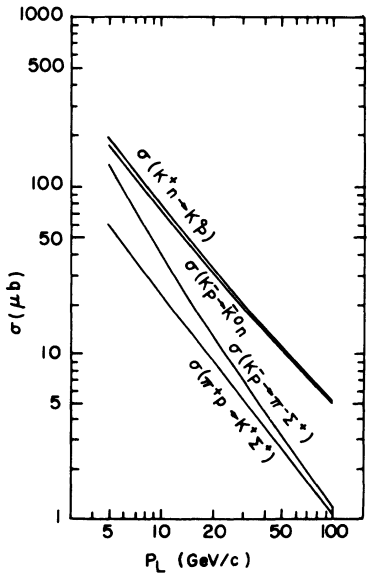

FIG. 10. Model results for the inelastic cross sections $\sigma(K^+n \to K^0p)$, $\sigma(K^-p \to \bar{K}^0n)$, $\sigma(K^-p \to \pi^-\Sigma^+)$, $\sigma(\pi^+p \to K^+\Sigma^+)$.

5. K^-p, K^+p charge exchange (CEX)

At lab momenta above 5 GeV/c, these reactions show little line-reversal breaking. In terms of our model, this is explained by the dominance of the helicity-flip amplitude in which there is no cut. The energy dependence of the cross sections for these reactions is given in Fig. 10. The line-reversal breaking is less than 5% above 10 GeV/c lab momentum. The KN CEX differential cross sections are shown in Fig. 11.

6. $\pi^-p \to \pi^0n$

The one remaining major discrepancy between our fit and the data is in the charge-exchange differential cross section beyond the dip, where the model is systematically low. We find that if agreement is forced by alteration of the residues or strengthening of the RP cut, then agreement with the hypercharge-exchange data deteriorates. The source of this problem might be anything from a simple inadequacy of the parametrization to a necessity for more extensive breaking of SU(3) than we have allowed. Note, however, that agreement is good for $|t| \lesssim 0.6$ (GeV/c)^2.

As previously discussed, the polarization is explained in terms of a destructive, predominantly imaginary cut in the helicity-nonflip amplitude together with an unabsorbed flip amplitude. The DCS and polarization data are shown in Fig. 12.

The energy dependences in our model of $\sigma(\pi^-p \to \pi^0n)$, $\Delta\sigma_{\text{tot}}(\pi p)$, and $d\sigma/dt\,(t=0)$ for $\pi^-p \to \pi^0n$ are $s^{-1.09}$, $s^{-0.37}$, and $s^{-0.91}$, respectively. These are to be compared with the experimentally determined values[66] $s^{-1.09}$, $s^{-0.31}$, and $s^{-0.84}$, respectively. The forward turnover near $t=0$ seen in Fig. 12 continues to be seen clearly in our model well past 100 GeV/c lab momentum, although the position of the turnover is about $-t = 0.01$ (GeV/c)^2.

The effective trajectory for this reaction is compared with the data[67] in Fig. 13. Note that the shrinkage continues well into the region past the signature zero. This is simply explained by the fact that the unabsorbed flip amplitude dominates the ρP cut completely in this region. The change in shape near $-t = 0.7$ (GeV/c)^2 is due to the slower shrinkage given by the ρP cut in a region where the pole amplitude is zero.

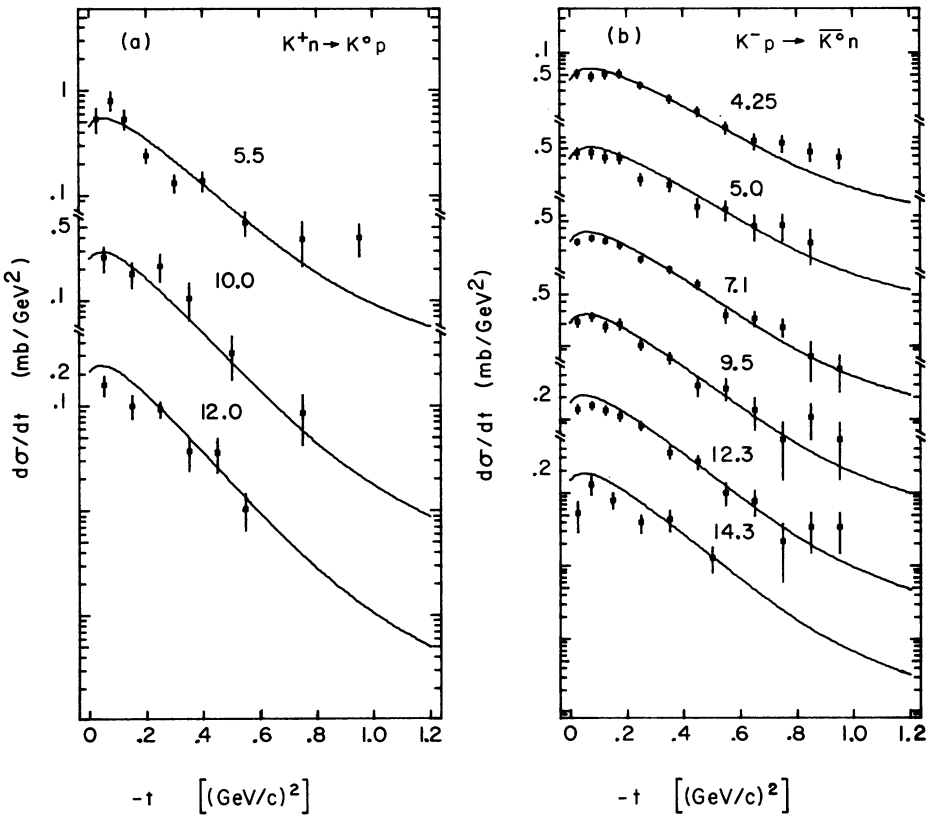

FIG. 11. Experimental measurements and model results of differential cross sections. (a) K^+n charge exchange (Refs. 31, 32, 34); (b) K^-p charge exchange (Refs. 29, 30, 33).

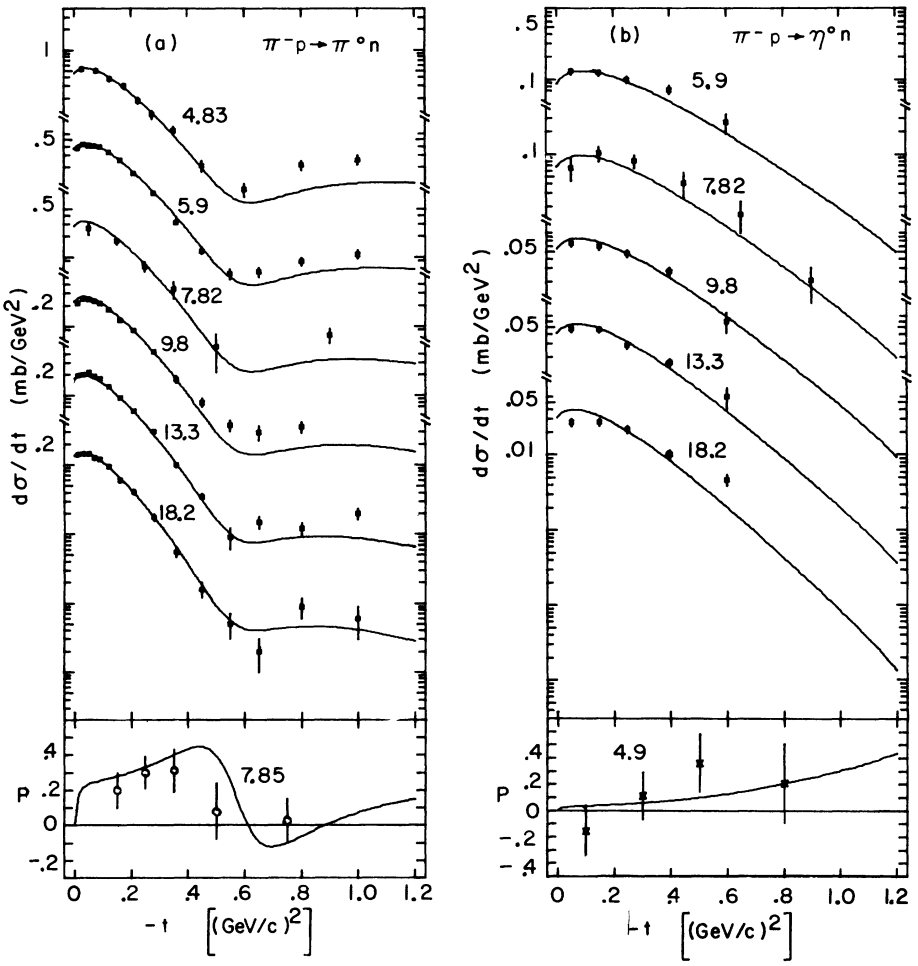

FIG. 12. Experimental measurements and model results for differential cross sections and polarizations. (a) $\pi^- p$ charge exchange (Refs. 24-28); (b) $\pi^- p \to \eta^0 n$ (Refs. 23-26). Not all the polarization data fitted are shown.

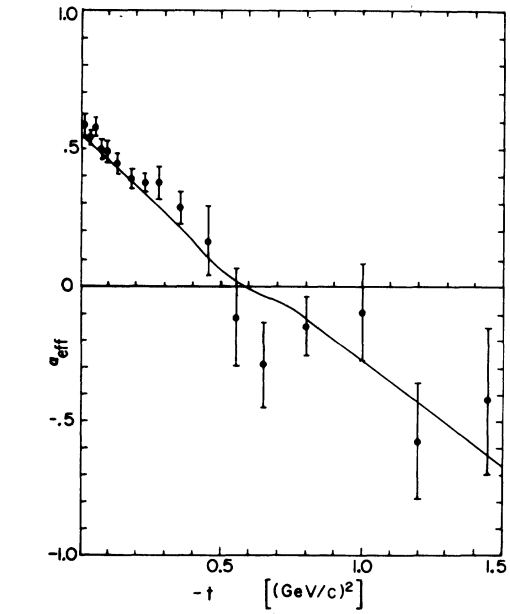

FIG. 13. Experimental measurements (Ref. 67) and model results for the effective trajectory for $\pi^- p \to \pi^0 n$.

7. $\pi^- p \to \eta n$

We find that mixing of the η must be taken into account in order to fit the magnitude of the differential cross sections. The theory is too large by several standard deviations when the η is treated as pure octet. After fitting the rest of the data, we used the singlet coupling strength given by duality[56] (and the quark model) and adjusted the mixing angle by inspection. The value we require is $\theta = 5°$, which is opposite in sign from the result of Martin and Michael.[68] These data are shown in Fig. 12.

8. $\pi^- p \to K^0 \Lambda$, $K^- n \to \pi^- \Lambda$, $K^- p \to \pi^0 \Lambda$

The polarizations and differential cross sections are reasonably well fitted down to 3 GeV/c. The slopes of the differential cross sections are somewhat smaller for the two exotic reactions, and our model also reproduces this feature.

Interpretation of the $\pi^- p \to K^0 \Lambda$ polarization is rather complicated, since the flip amplitude is not purely real. The data for this reaction and $\pi^+ p$

$\rightarrow K^+\Sigma^+$, which is theoretically similar, both indicate a sign change at $|t| \approx 0.25$ (GeV/c)^2, after which point the polarization takes the sign contributed by the destructive imaginary part of the K^* cut. In terms of the model, this sign change arises from the real part of the cut, to which the constructive real part in $K^* \otimes P$ and the destructive real part in $K^{**} \otimes P$ add constructively. At small t, the imaginary part of the flip amplitude is dominant, so the real part of the cut dominates the polarization. However, the imaginary part of flip decreases rapidly and changes sign at $t \approx -0.4$ (GeV/c)^2, while the real part does not change sign, so for $|t| \gtrsim 0.25$ (GeV/c)^2 the imaginary part of the cut dominates the polarization, and for $|t| \gtrsim 0.4$ (GeV/c)^2, the two contributions have the same sign.

This sign change seems definitely to be present in both the $\pi^- p \rightarrow K^0\Lambda$ and $\pi^+ p \rightarrow K^+\Sigma^+$ data, and might be regarded as evidence against the similarity of ρ and K^* cuts if the explanation above, requiring an appreciable real part in the K^* cut is correct.

As previously discussed, the exotic polarizations can be explained as arising from the destructive imaginary part of the K^* cut. These data are shown in Fig. 14.

9. $\pi^+ p \rightarrow K^+\Sigma^+$, $K^- p \rightarrow \pi^-\Sigma^+$

In addition to the line-reversal breaking present in these reactions, a very noticeable feature of the differential cross sections is a distinct change of slope at about $|t| = 0.5$ (GeV/c)^2 for the reaction with rotating phase. The slope change is also present in $\pi^- p \rightarrow K^0\Lambda$ and $\pi^- p \rightarrow K^0\Sigma^0$ (Fig. 15). In our model, this break is the result of a sharp dip in the contribution to the DCS from the nonflip amplitude. The dip is not related to a signature zero, but instead is the result of a strong destructive real part of the RP cut causing a near coincidence of the zeros in the real and imaginary parts of the nonflip amplitude.

The polarization for $\pi^+ p \rightarrow K^+\Sigma^+$ has been dis-

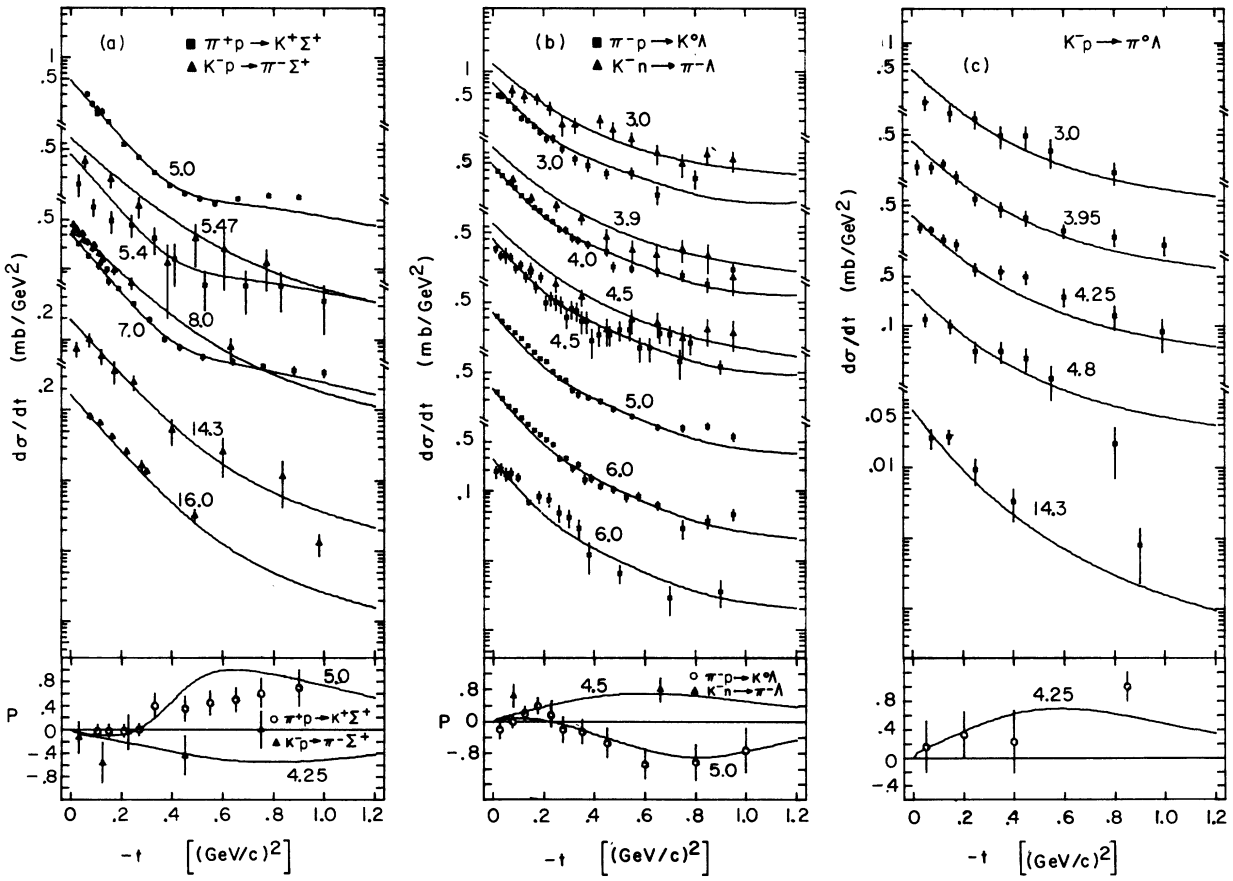

FIG. 14. Experimental measurements and model results for differential cross sections and polarizations. (a) $\pi^+ p \rightarrow K^+\Sigma^+$ (Refs. 45–47), $K^- p \rightarrow \pi^-\Sigma^+$ (Refs. 29, 33, 42–44); (b) $\pi^- p \rightarrow K^0\Lambda$ (Refs. 35 and 36), $K^- n \rightarrow \pi^-\Lambda$ (Refs. 38–40); (c) $K^- p \rightarrow \pi^0\Lambda$ (Refs. 29, 33, 41, 42).

cussed in Sec. V B 8, and the polarization for the exotic reaction $K^-p \to \pi^-\Sigma^+$ has also been discussed at some length in Sec. III. Both are well reproduced by the model. In both reactions, however, we are unable to fit the differential cross-section magnitudes below 5.0 GeV/c. We do fit $\pi^-p \to K^0\Sigma^0$, which is related by t-channel isospin to $\pi^+p \to K^+\Sigma^+$ down to 3.0 GeV/c. For both reactions, the model results are too large at the lower energies. These data are presented in Fig. 14. The expected behavior of the cross sections for the line-reversed pair $\pi^+p \to K^+\Sigma^+$ and $K^-p \to \pi^-\Sigma^+$ is given in Fig. 10. The line-reversal breaking remains substantial (~20%) even at 100 GeV/c.

10. $K^+p \to \eta\Lambda$, $K^-p \to \eta'\Lambda$

For $K^-p \to \eta\Lambda$, the data indicate a pronounced dip at $|t| \approx 0.4$ (GeV/c)^2. In the absence of mixing, the pole part of the amplitude is given by $A \sim K^{**} + 3K^*$, so the dip can be attributed to the signature zero in the dominant K^*-exchange amplitude. As shown in Fig. 16, our model agrees only roughly with the data. Contributions from the cut and the K^{**} amplitude are sufficient to fill in the dip and give instead a very sharp break in slope. Agreement with the featureless shape of $K^-p \to \eta'\Lambda$ is reasonable.

It should be noted that the η-η' mixing angle, which affects the differential cross-section magnitudes for these reactions, was determined solely from the $\pi^-p \to \eta^0 n$ data.

C. Amplitudes

Since considerable polarization is observed in several reactions which are exotic according to duality diagrams, one obviously cannot say that the amplitudes corresponding to nonplanar duality diagrams are purely real. However, if our model results are taken seriously, one can make the following statements:

(1) The flip amplitude corresponding to a nonplanar diagram is purely real, while the amplitude for a planar diagram has phase $e^{-i\pi\alpha}$.

(2) The nonflip amplitude corresponding to a planar diagram has a peripheral imaginary part

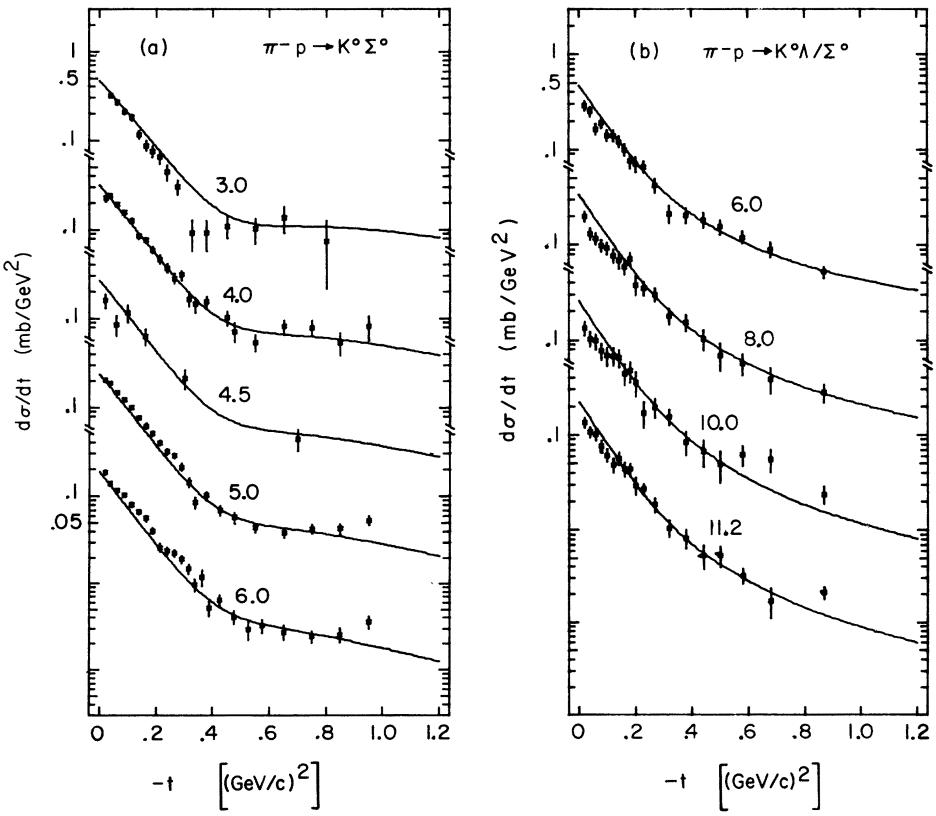

FIG. 15. Experimental measurements and model results for differential cross sections. (a) $\pi^-p \to K^0\Sigma^0$ (Refs. 35 and 36); (b) $\pi^-p \to K^0\Lambda/\Sigma^0$ (Ref. 37).

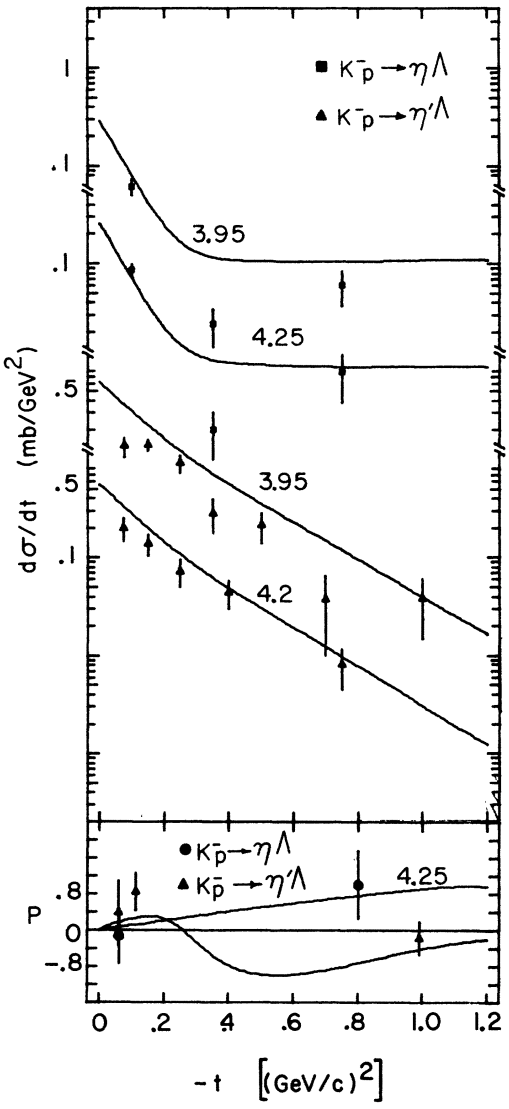

FIG. 16. Experimental measurements and model results for differential cross sections and polarizations in the reactions $K^-p \to \eta\Lambda$ and $K^-p \to \eta'\Lambda$ (Refs. 29 and 48).

with the same zeros as given by the dual absorption model. For a nonplanar diagram, the nonflip amplitude has a structureless, nonperipheral imaginary part which does not change sign for $|t| \lesssim 1.5$ $(\mathrm{GeV}/c)^2$, and the real to imaginary ratio at $t=0$ is a factor of 3–5 larger than is the case for planar amplitudes.

The structure of our exotic helicity-nonflip amplitudes is considerably different from that obtained in a recent amplitude analysis[58] based on the dual absorption model.[63] In that analysis, both vector- and tensor-exchange amplitudes were taken to be peripheral. While the K^+n charge-exchange amplitude (which is quark-model exotic) was found to have a small imaginary part, amplitudes for processes which are exotic only by duality diagrams were found to be similar in structure to their line-reversed counterparts, with large, peripheral imaginary parts. Since both models reproduce the polarization data, measurements of the spin rotation parameters will be required to determine which, if either, picture is correct. Some of the amplitudes are shown in Figs. 17 and 18.

D. Comparison with the classical absorption model

Just as the present work was nearing completion, a new version of the strong absorption model appeared in a paper by Hartley and Kane.[59] This model, called the classical absorption model (CAM) by its authors has been applied to a large amount of $0^-\frac{1}{2}^+$ data in a fashion similar to the present paper.

At intermediate energies (3–15 GeV) both models reproduce the known πN amplitudes, and therefore both models give good descriptions [via SU(3)] of all $0^-\frac{1}{2}^+$ reactions in the intermediate-energy range. The main differences between the two models in this energy region are the signs of many inelastic polarizations in the region $-1.5<t<-0.4$ $(\mathrm{GeV}/c)^2$; unfortunately, the existing data are not of sufficient quality to decide the true behavior of the polarizations.

These sign differences in the polarizations are presumably due to absorption effects in tensor amplitudes in the CAM which the authors claim are highly sensitive to the details of absorption in the model. By contrast, our tensor amplitudes are hardly absorbed at all and depend only on the exchange degeneracy which follows from duality for pole amplitudes.

At moderately high momenta (20–60 GeV/c), inelastic cross-section data should provide rather clear distinctions between the two models. For example, the CAM predicts $\sigma(K^+n \to K^0p)/\sigma(K^-p \to \overline{K}^0n) \sim 1.5$ over a wide range of momenta above 20 GeV/c. If such is indeed the case, our model would require the appearance in the helicity-flip amplitude of some absorption which was not present at intermediate energies. Line-reversal breaking in hypercharge exchange reactions will presumably not provide a clear distinction between the two models, since we predict $\sigma(K^-p \to \pi^-\Sigma^+)/\sigma(\pi^+p \to K^+\Sigma^+) \sim 1.4$ and ~ 1.23 at the momenta 25 and 60 GeV/c, respectively. Generally we expect no drastic changes in the structure of the inelastic polarizations in the range 20–60 GeV/c; the CAM apparently predicts a return to the structures previously associated with the old strong-absorption model.

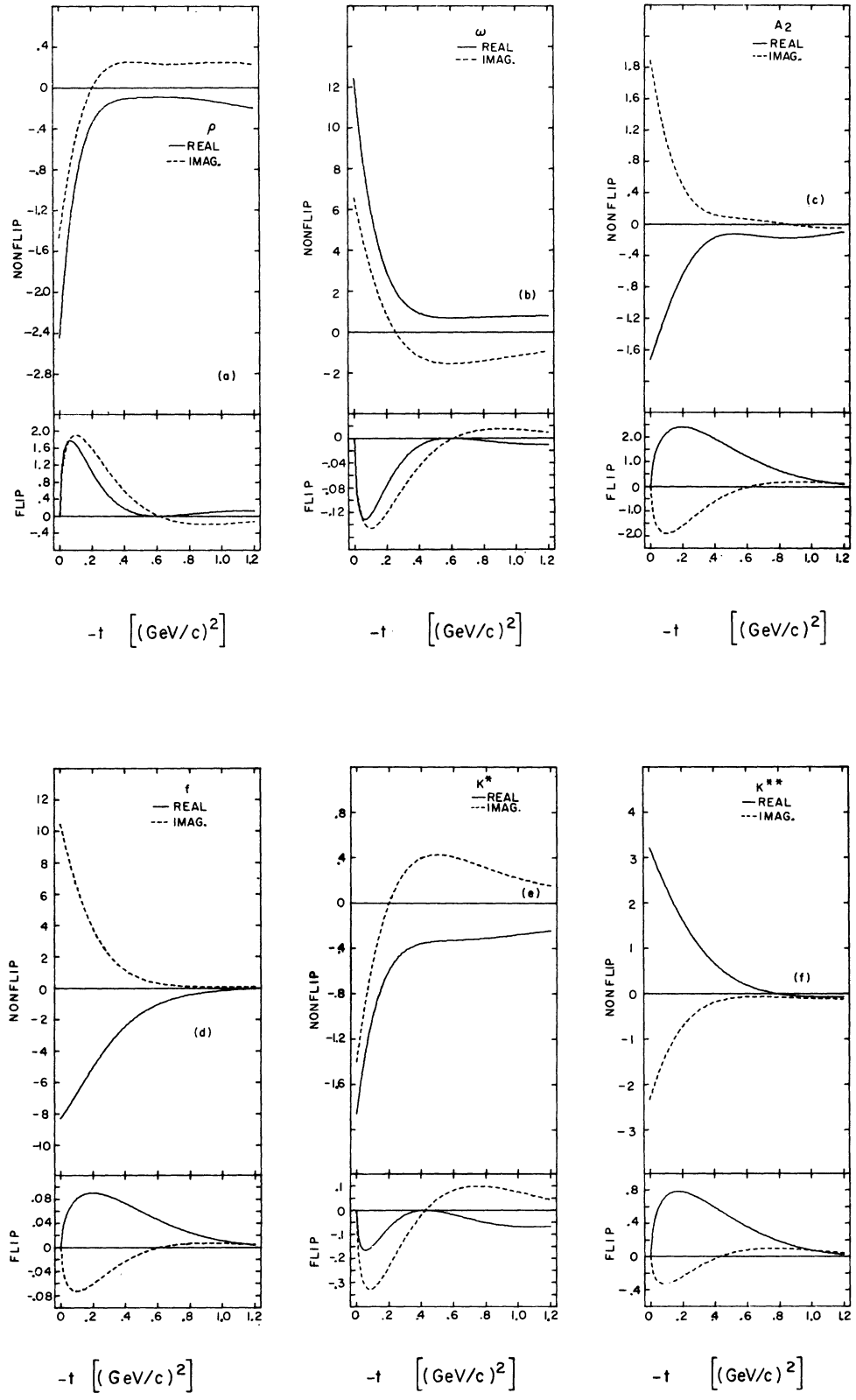

FIG. 17. Model results for individual particle exchange amplitudes at 6.0 GeV/c.

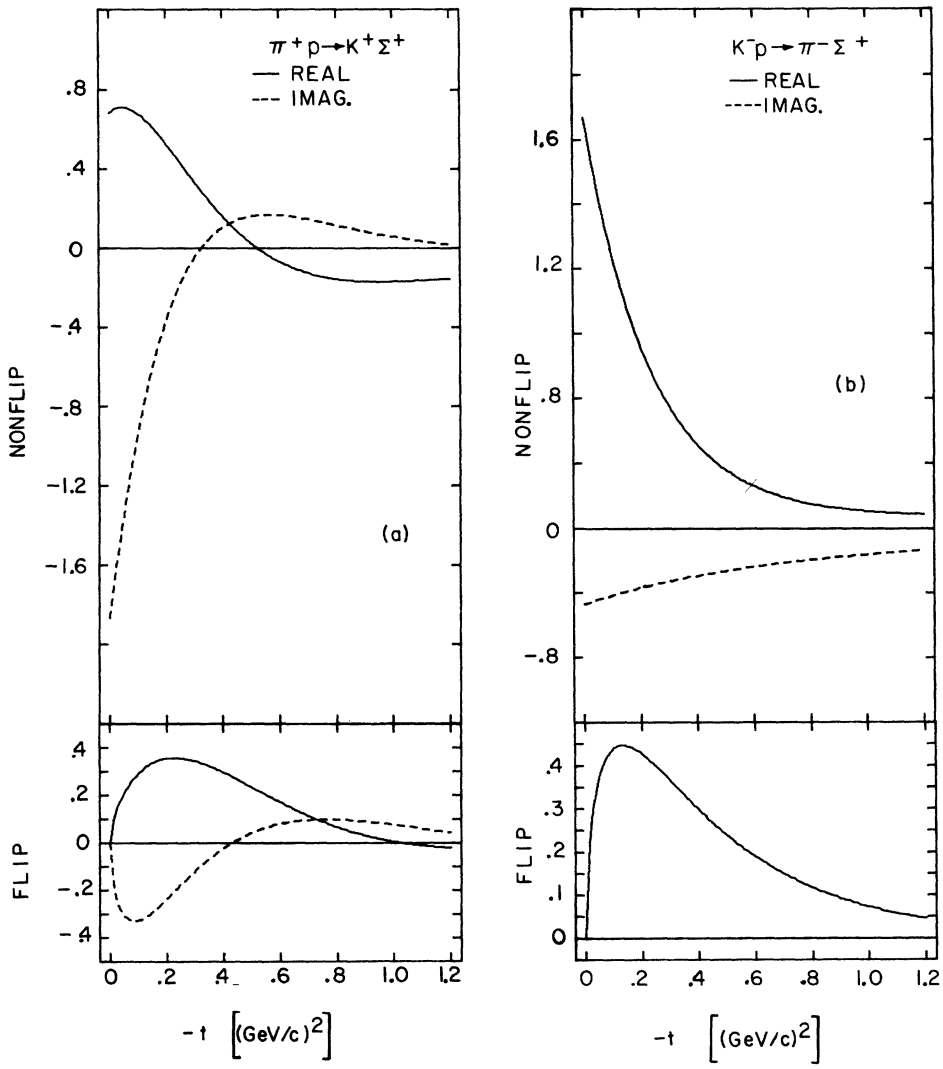

FIG. 18. Model results for the total (pole plus cut) helicity-nonflip and -flip amplitudes for the line-reversed pair of reactions (a)$\pi^+p \to K^+\Sigma^+$; (b) $K^-p \to \pi^-\Sigma^+$.

Our model, based on duality and SU(3) symmetry, stresses simplicity, both physically and conceptually. Exchange degeneracy for pole amplitudes is a theorem following directly from duality and the absence of exotic particles. We stress that in any general overview of $0^-\frac{1}{2}^+$ reactions based on EXD amplitudes, the only deviation from the basic input physics occurs when the imaginary part of the vector amplitude is absorbed. We consider this deviation, admittedly not fundamentally understood, a minor price to pay for the highly quantitative description of $0^-\frac{1}{2}^+$ data obtained in the present work.

The classical absorption model, on the other hand, emphasizes a proposed complexity, supposedly due to a very strong role being played by unitarity. This complexity is formulated in terms of ideas based on the collective effects of many terms in the s-channel unitarity sum, and is parametrized by a vacuum amplitude which apparently has no simple connection with Regge poles. Absorption with this vacuum amplitude is the major force in the CAM, so the output amplitudes bear no resemblance whatsoever to the input poles. In the CAM duality is just an intermediate-energy accident. No evidence is offered by the CAM as to why such an accident should occur.

Both the present model and the CAM achieve quantitative success, but only at the price of introducing *ad hoc* ingredients in both cases. In our model, the *ad hoc* factor is the Ringland phase modification, which we showed was equivalent

to the assumption that only imaginary parts in vector amplitudes are absorbed if the input poles are exchange degenerate. Thus if we count real and imaginary parts of vector and tensor amplitudes, both flip and nonflip, as eight basic ingredients of the input physics, only one of these ingredients is significantly changed, and it is changed about 25%. In the CAM, the *ad hoc* factor is the proposed vacuum amplitude. Since the absorption is strong, none of the output amplitudes is similar to its input pole. Thus even the qualitative success of the CAM depends crucially on the strong effects of an *ad hoc* ingredient in the model.

E. Some technical aspects of the fit

In this section we wish to discuss briefly the statistical quality of our analysis. The χ^2 per data point for the fitted result presented is 2.6 for 1987 data points. We remark that this χ^2 reflects not only the deviation of our model from the parent distribution function, but also the deviation of the data from the parent distribution. When one analyzes 143 different experiments simultaneously, the total effect of systematic errors can become comparable to the statistical errors. By varying the normalization of each experiment within the systematic errors quoted by the authors, we determined that about one third of the χ^2 may come from systematic errors. However, since the average of all renormalizations was very nearly zero, and since none of the parameters was seriously affected, we chose to ignore these errors during our final analysis. We hope that experimentalists will soon consider it worthwhile to refine our knowledge by repeating many important experiments in the intermediate-energy range (3–30 GeV/c) with higher statistics and smaller systematic errors.

VI. CONCLUSION AND SUMMARY

We have presented a model that describes nearly all high-energy data for reactions of the type $0^-\frac{1}{2}^+ \to 0^-\frac{1}{2}^+$. The description obtained is qualitatively and, in most cases, quantitatively excellent. It has been known for some time that each of the major hypotheses of the model cooperates in an unusually elegant fashion to provide a description of these data that is both simple and complete. These hypotheses are SU(3) symmetry for all amplitudes, except as broken by inequality of the strange and nonstrange trajectories and the octet part of the Pomeron, Regge dominance of amplitudes above 3.0 GeV/c, and duality and absence of exotics in the reations $0^-0^- \to 0^-0^-$ and $0^-\frac{1}{2}^+ \to 0^-\frac{1}{2}^+$, implying strong exchange degeneracy for the Regge-*pole* amplitudes ρ–ω–A_2–f and K^*–K^{**}. The RP cuts then provide imaginary parts that break exchange degeneracy for the amplitudes. We have seen no indication from this analysis that any of these hypotheses is not consistent with the present experimental knowledge of the reactions being considered.

In addition, we made some technical assumptions in the interest of simplicity and facility. For example, these include absence of RP cuts in the helicity-flip amplitude, absence of RR cuts and secondary meson trajectories, and absence of effects such as RPP and $RPPP$ cuts. These assumptions can of course be relaxed at the expense of introducing more freedom into the model.

It is apparent that the one other important factor in our model is the Ringland phase modification. As discussed in detail in Secs. III and IV, this phase modification is directly responsible for correlating inelastic polarizations and DCS line-reversal breaking. We have implemented the modification in crossing-symmetric form, and have shown that it is equivalent to other methods of modifying the absorptive cut; in particular, one can think of absorbing vector exchanges more strongly than tensor exchanges, or one can think of absorbing the $e^{-i\pi\alpha}$ term more strongly than the 1 term in the Regge signature factor. Our results are not consistent with the dual absorptive model assumption that tensor exchanges are peripheral. Even though the Ringland modification is somewhat *ad hoc*, it apparently is an unavoidable consequence of a large amount of data, when these data are viewed from a simple theoretical framework (see, however, Ref. 59). Unfortunately, there is still a major gap in our fundamental understanding of the modification.

This work should be regarded as a highly model-dependent high-energy amplitude analysis. We note that except for the Pomeron trajectory slope α'_P every parameter is in a t-dependent residue, and we have no *a priori* knowledge about these residue functions. Each of the parameters is influencing many reactions. For example, only one parameter is responsible for all deviations from SU(3) and duality for all πN and KN elastic scatterings. The same Pomeron that dominates these elastic scatterings is used to calculate the RP cut in each of 12 different inelastic reactions, both hypercharge and nonhypercharge exchange. SU(3) gives the relative amount of RP cut in each reaction, implying that SU(3) works as well for cuts as for poles.

The classical absorption model provides an interesting and serious alternative to the points of view that we have presented here. Ideally, good experimental evidence will help decide which (if either) approach is correct. Unfortunately, a review of the past history of this subject does not encourage such an idealistic hope in our opinion.

APPENDIX

If we number the states of the octet as shown in Fig. 19, the matrices appropriate to Eqs. (1)–(3) are

$$M_1=\begin{vmatrix}0&-1&0\\0&0&0\\0&0&0\end{vmatrix}, \quad M_2=\begin{vmatrix}0&0&-1\\0&0&0\\0&0&0\end{vmatrix},$$

$$M_3=\begin{vmatrix}0&0&0\\0&0&-1\\0&0&0\end{vmatrix}, \quad M_4=\begin{vmatrix}0&0&0\\1&0&0\\0&0&0\end{vmatrix},$$

$$M_5=\begin{vmatrix}0&0&0\\0&0&0\\1&0&0\end{vmatrix}, \quad M_6=\begin{vmatrix}0&0&0\\0&0&0\\0&-1&0\end{vmatrix},$$

$$M_7=(\tfrac{1}{2})^{1/2}\begin{vmatrix}1&0&0\\0&-1&0\\0&0&0\end{vmatrix}, \quad M_8=(\tfrac{1}{6})^{1/2}\begin{vmatrix}1&0&0\\0&1&0\\0&0&-2\end{vmatrix}.$$

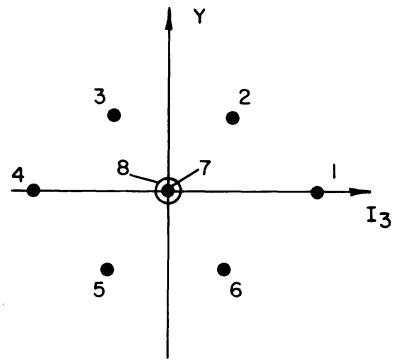

FIG. 19. Numbering of the octet states.

According to Eq. (1), the SU(3) Clebsch-Gordan coefficient for the symmetric coupling of $p\overline{K}^*$ to Σ^+ is given by

$$\langle p,\overline{K}^{*0}|\Sigma^+\rangle=(\tfrac{3}{10})^{1/2}\langle \tilde{M}_1\{M_2,M_6\}\rangle$$
$$=-(\tfrac{3}{10})^{1/2}.$$

---

*Based in part on work submitted to Iowa State University by S. E. Egli in partial fulfillment of the requirements for the Ph.D. degree.

[1]A. Citron *et al.*, Phys. Rev. 144, 1101 (1966).
[2]K. Foley *et al.*, Phys. Rev. Lett. 19, 330 (1967).
[3]S. Denisov *et al.*, Phys. Lett. 36B, 530 (1971).
[4]K. Foley *et al.*, Phys. Rev. 181, 1775 (1969).
[5]I. Ambats *et al.*, Phys. Rev. Lett. 29, 1415 (1972).
[6]K. Foley *et al.*, Phys. Rev. Lett. 11, 425 (1963).
[7]D. Harting *et al.*, Nuovo Cimento 38, 60 (1965).
[8]Yu. Antipov *et al.*, presented to the XVI International Conference on High Energy Physics, Chicago-Batavia, Ill., 1972 (unpublished).
[9]A. Derevitchikov *et al.*, presented to the XVI International Conference on High Energy Physics, Chicago-Batavia, Ill., 1972 (unpublished).
[10]M. Borghini *et al.*, Phys. Lett. 31B, 405 (1970).
[11]M. Borghini *et al.*, Phys. Lett. 36B, 493 (1971).
[12]A. DeLesquen *et al.*, Phys. Lett. 40B, 277 (1972).
[13]A. Diddens *et al.*, Phys. Rev. 132, 2722 (1963).
[14]W. Galbraith *et al.*, Phys. Rev. 138, B913 (1965).
[15]L. Schroeder *et al.*, Phys. Rev. 176, 648 (1968).
[16]K. Foley *et al.*, Phys. Rev. Lett. 11, 503 (1963).
[17]K. Foley *et al.*, Phys. Rev. Lett. 15, 45 (1965).
[18]M. Borghini *et al.*, Phys. Lett. 36B, 497 (1971).
[19]J. Allaby *et al.*, Phys. Lett. 30B, 500 (1969).
[20]S. Denisov *et al.*, Phys. Lett. 36B, 415 (1971).
[21]W. Baker *et al.*, Phys. Rev. 129, 2285 (1963).
[22]P. Jain *et al.*, Nucl. Phys. B19, 568 (1970).
[23]O. Guisan *et al.*, Phys. Lett. 18, 200 (1965).
[24]O. Guisan *et al.*, Nucl. Phys. B32, 681 (1971).
[25]P. Bonamy *et al.*, Nucl. Phys. B52, 392 (1973).
[26]P. Bonamy *et al.*, Nucl. Phys. B16, 335 (1970).
[27]P. Sonderegger *et al.*, Phys. Lett. 20, 75 (1966).
[28]A. Stirling *et al.*, Phys. Rev. Lett. 14, 763 (1965).
[29]R. Blokzijl *et al.*, Nucl. Phys. B51, 535 (1973).
[30]P. Astbury *et al.*, Phys. Lett. 23, 396 (1966).
[31]D. Cline *et al.*, Nucl. Phys. B22, 247 (1970).
[32]M. Haguenauer *et al.*, Phys. Lett. 37B, 538 (1971).
[33]R. J. Miller *et al.*, presented to the XVI International Conference on High Energy Physics, Chicago-Batavia, Ill., 1972 (unpublished).
[34]A. Firestone *et al.*, Phys. Rev. Lett. 25, 958 (1970).
[35]C. Ward *et al.*, private communication.
[36]K.-W. Lai *et al.*, Phys. Rev. D 6, 1220 (1972).
[37]E. Bertolucci *et al.*, Nuovo Cimento Lett. 2, 149 (1969).
[38]R. Barloutaud *et al.*, Nucl. Phys. B9, 493 (1969).
[39]D. Crennell *et al.*, Phys. Rev. Lett. 23, 1347 (1969).
[40]W. Yen *et al.*, Phys. Rev. 188, 2011 (1969).
[41]M. Aguilar-Benitez *et al.*, Phys. Rev. D 6, 29 (1972).
[42]L. Moscoso *et al.*, Nucl. Phys. B36, 332 (1972).
[43]J. Loos *et al.*, Phys. Rev. 173, 1330 (1968).
[44]D. Birnbaum *et al.*, Phys. Lett. 31B, 484 (1970).
[45]S. Pruss *et al.*, Phys. Rev. Lett. 23, 189 (1969).
[46]S. Pruss *et al.*, Phys. Rev. Lett. 27, 74 (1971).
[47]W. Cooper *et al.*, Phys. Rev. Lett. 20, 472 (1968).
[48]L. Moscoso *et al.*, Phys. Lett. 40B, 285 (1972).
[49]F. Henyey, G. L. Kane, J. Pumplin, and M. H. Ross, Phys. Rev. 182, 1579 (1969).
[50]R. C. Arnold, Phys. Rev. 153, 1523 (1967).
[51]P. D. B. Collins, Phys. Rep. 1, 103 (1971).
[52]V. Barger and R. J. N. Phillips, Phys. Rev. 187, 2210 (1969).
[53]R. Hong Tuan, J. M. Kaplan, and G. Sanguinetti, Nucl. Phys. B32, 165 (1971).
[54]A. C. Irving, A. D. Martin, and C. Michael, Nucl. Phys. B32, 1 (1971).
[55]G. A. Ringland, R. G. Roberts, D. P. Roy, and T. Tran Thanh Van, Nucl. Phys. B44, 395 (1972).

[56]D. Barkai and K. J. M. Moriarty, Nucl. Phys. B50, 354 (1972).
[57]B. Sadoulet, Nucl. Phys. B53, 135 (1973).
[58]J. S. Loos and J. A. J. Matthews, Phys. Rev. D 6, 2463 (1972).
[59]B. J. Hartley and G. L. Kane, Nucl. Phys. B57, 157 (1973).
[60]M. Imachi, T. Matsuoka, K. Ninomiya, and S. Sawada, Progr. Theor. Phys. 40, 353 (1968); H. Harari, Phys. Rev. Lett. 22, 562 (1969); J. Rosner, *ibid.* 22, 689 (1969).
[61]J. Mandula, J. Weyers, and G. Zweig, Annu. Rev. Nucl. Sci. 20, 289 (1970).
[62]G. Cohen-Tannoudji, A. Morel, and Ph. Salin, Nuovo Cimento 55A, 412 (1969).
[63]M. Davier and H. Harari, Phys. Lett. 35B, 239 (1971).
[64]G. C. Fox and C. Quigg, LBL Report No. 20001, 1970 (unpublished).
[65]B. B. Brabson *et al.*, Phys. Rev. Lett. 25, 553 (1970).
[66]V. N. Bolotov *et al.*, Phys. Lett. 38B, 120 (1972).
[67]G. Höhler *et al.*, Phys. Lett. 20, 79 (1966).
[68]A. D. Martin and C. Michael, Phys. Lett. 37B, 513 (1971).

PHYSICAL REVIEW D VOLUME 9, NUMBER 5 1 MARCH 1974

Analysis of $\bar{p}p$ interactions and the quark-parton model*

A. E. Bussian†
Randall Laboratory of Physics, University of Michigan, Ann Arbor, Michigan 48104
(Received 13 February 1973)

An analysis of $\bar{p}p$ interactions is made assuming that hadrons are composed of totally absorbing subparticles. If quarks are assumed to be the basic constituents, their mass and radius are in reasonable agreement with the Drell-Johnson model. If the subparticles are assumed to be Schwarzschild spheres, the resulting mass and radius agree with Planck's characteristic mass and length, respectively. Furthermore, the resulting mass density of partons is of the correct order of magnitude to be gravitationally bound into nucleons.

In recent years composite models of hadrons have been constructed to explain high-energy phenomena. Such entities as quarks, partons, and droplets have been proposed as the basic constituents of hadrons. For convenience we shall refer to partons as any basic subunits of hadronic matter.

In this paper $\bar{p}p$ interactions are analyzed, assuming such a composite picture in terms of the impact representation of the optical model. $\bar{p}p$ interactions are particularly amenable to such a study because of the apparent pure imaginary scattering amplitude at finite energies[1] and the absence of discrete $\bar{p}p$ resonances. Within this framework a number of authors have considered pp elastic scattering in the asymptotic energy limit where the real part of the amplitude is expected to be zero.[2] Measured differential cross sections appear to approach this limit with increasing energy.

The partial-wave expansion of the imaginary part of the scattering amplitude, neglecting spin, is given by

$$f(\theta)=\frac{1}{2ik}\sum_{l=0}^{\infty}(2l+1)\{\exp[-\alpha(k)g_l(k)]-1\}\times P_l(\cos\theta)\,, \tag{1}$$

where the absorption coefficient has been written as a product of two factors. Expressions for cross sections are given by

$$\sigma_e=\frac{\pi}{k^2}\sum_{l=0}^{\infty}(2l+1)\{1-\exp[-\alpha(k)g_l(k)]\}^2\,, \tag{2}$$

$$\sigma_t=\frac{2\pi}{k^2}\sum_{l=0}^{\infty}(2l+1)\{1-\exp[-\alpha(k)g_l(k)]\}\,, \tag{3}$$

$$\frac{d\sigma}{dt}=\frac{\pi}{P_{\text{c.m.}}^{\,2}}|f(\theta)|^2\,. \tag{4}$$

The transformation to the impact-parameter representation is usually given by[3]

$$l+\tfrac{1}{2}=kb\,. \tag{5}$$

Using (5) one can transform $g_l(k)\to g(b)$, where $g(b)$ takes into account the density distribution of two hadrons which are passing through each other at impact parameter b and is given by

$$g(b)=\int_{x_{\min}}^{x_{\max}}\int_{y_{\min}}^{y_{\max}}\int_{0}^{z_{\max}}\int_{0}^{w_{\max}}\rho_B(x,y,z)\rho_T(x,y,w)\times dw\,dz\,dy\,dx\,. \tag{6}$$

ρ_B (ρ_T) is the beam (target) particle hadronic matter distribution normalized to one parton. The w and z coordinate axes are in the direction of the beam particle.